Acta Pharmaceutica Sinica B 2022;12(1):437−450

Chinese Pharmaceutical Association
Institute of Materia Medica, Chinese Academy of Medical Sciences

Acta Pharmaceutica Sinica B

www.elsevier.com/locate/apsb
www.sciencedirect.com

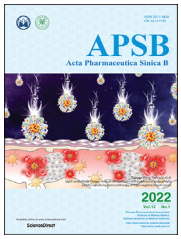

ORIGINAL ARTICLE

A real-time and modular approach for quick detection and mechanism exploration of DPIs with different carrier particle sizes

Yingtong Cui[a,b,†], Ying Huang[a,b,†], Xuejuan Zhang[a,b,*], Xiangyun Lu[c], Jun Xue[d], Guanlin Wang[b], Ping Hu[a], Xiao Yue[b], Ziyu Zhao[b,e], Xin Pan[b,*], Chuanbin Wu[a,b]

[a]*School of Pharmaceutical Science, Jinan University, Guangzhou 510006, China*
[b]*School of Pharmaceutical Sciences, Sun Yat-sen University, Guangzhou 510006, China*
[c]*Micromeritics Instrument (Shanghai) Ltd., Shanghai 200135, China*
[d]*MEGGLE Group Shanghai Representative Office, Shanghai 201315, China*
[e]*Department of Pharmacology, Zhongshan School of Medicine, Sun Yat-sen University, Guangzhou 510080, China*

Received 6 February 2021; received in revised form 9 April 2021; accepted 6 May 2021

KEY WORDS

Dry powder inhaler;
Carrier particle size;
Pulmonary delivery process;
Real-time monitor;
Quick detection

Abstract Dry powder inhalers (DPIs) had been widely used in lung diseases on account of direct pulmonary delivery, good drug stability and satisfactory patient compliance. However, an indistinct understanding of pulmonary delivery processes (PDPs) hindered the development of DPIs. Most current evaluation methods explored the PDPs with over-simplified models, leading to uncompleted investigations of the whole or partial PDPs. In the present research, an innovative modular process analysis platform (MPAP) was applied to investigate the detailed mechanisms of each PDP of DPIs with different carrier particle sizes (CPS). The MPAP was composed of a laser particle size analyzer, an inhaler device,

Abbreviation: AE, aerated energy; APIs, active pharmaceutical ingredients; AR, aeration ratio; BFE, basic flow Energy; CFD-DEM, computational fluid dynamics-discrete element method; C.OPT, optical concentration; CPS, carrier particle size; d_{ae}, aerodynamic diameter; DPIs, dry powder inhalers; dQ_3, the volume percentage of particles within certain range; ED, emitted dose; EDXS, energy-dispersive X-ray spectroscopy; F_C, centrifugal force; F_D, drag force; F_F, friction force; F_G, gravity; F_I, interaction force; F_P, press-on force; FPD, fine particle dose; FPF, fine particle fraction; FT4, Freeman Technology 4; HPLC, high performance liquid chromatography; HPMC, hydroxypropyl methyl cellulose; LAC, lactose; MFV, minimum fluidization velocity; MMAD, mass median aerodynamic diameter; MOC, micro orifice collector; MPAP, modular process analysis platform; MSS, micronized salbutamol sulfate; NGI, Next Generation Impactor; O, oxygen; PD, pressure drop; PDP, pulmonary delivery process; PSF, particle size fractions; R_{AUC}, total release amount; R_{max}, maximum of release amount; R, release amount; S, stopping distance; SE, specific energy; SEM, scanning electron microscope; SSA, specific surface area; T_{max}, the time to reach R_{max}; T_t, terminal time; T, time; TE, total engery; U_0, air flow rate; V_0, velocity.

*Corresponding authors. Tel./fax: +86 20 39943115.
E-mail addresses: zhanghongdou0223@126.com (Xuejuan Zhang), panxin2@mail.sysu.edu.cn (Xin Pan).
†These authors made equal contributions to this work.

Peer review under responsibility of Chinese Pharmaceutical Association and Institute of Materia Medica, Chinese Academy of Medical Sciences.

https://doi.org/10.1016/j.apsb.2021.06.011

an artificial throat and a pre-separator, to investigate the fluidization and dispersion, transportation, detachment and deposition process of DPIs. The release profiles of drug, drug aggregation and carrier were monitored in real-time. The influence of CPS on PDPs and corresponding mechanisms were explored. The powder properties of the carriers were investigated by the optical profiler and Freeman Technology four powder rheometer. The next generation impactor was employed to explore the aerosolization performance of DPIs. The novel MPAP was successfully applied in exploring the comprehensive mechanism of PDPs, which had enormous potential to be used to investigate and develop DPIs.

1. Introduction

Dry powder inhalers (DPIs) had raised extensive attention in the world, allowing directly administration to deep lung for high local drug concentrations[1], and systematic drug absorption without first-pass effect[2]. However, insurmountable technical barriers due to lacking of fundamental process-related theories, high cost and long production cycle had restricted the development of DPIs. A few studies roughly summarized the pulmonary delivery processes (PDPs) of DPIs, which could be divided into four processes (Fig. 1): fluidization and dispersion of DPIs in the inhaler device, transportation of DPIs through oropharynx and throat, detachment of APIs from the carriers[3,4] in bronchi and deposition of APIs in the lung[5]. However, the detailed mechanism of PDPs was unclear owing to the lack of efficient evaluation approaches, so the gap between the theories and the DPIs development still existed.

In general, the most common evaluation approaches of PDPs were Next Generation Impactor (NGI, Copley Scientific Ltd., Nottingham, UK) and computational fluid dynamic-discrete element method (CFD-DEM). NGI was widely recognized by the pharmacopoeia of several countries[6–8]. The common indicators such as aerodynamic diameter (d_{ae}), fine particle fraction (FPF), fine particle dose (FPD), emitted dose (ED), mass median aerodynamic diameter (MMAD) values and drug deposition profiles could be obtained by NGI[9], which served as indicators of aerosolization performance of DPIs. Nevertheless, only the final deposition state of DPIs could be detected by NGI instead of real-time monitoring, so it was hard to provide more detailed information for the PDPs of DPIs. Moreover, it was time and labor consuming to conduct NGI tests since the complicated operation and followed up quantification required an entire day for only one measurement, and thus severely hampered the efficiency of the industrialization processes. CFD-DEM model was a powerful tool to simulate the behavior of fluid–particle interactions[10], and was successfully employed in DPIs to aid the analyzing particle motion in the inhaler devices[11], throat[12] and bronchi 3D models[13,14]. However, the crucial physical properties, such as the particle shape, surface roughness and particle size distribution, were often over simplified in CFD-DEM model. In addition, the model development was a drawn-out process. Moreover, most of the CFD-DEM models only focused on partial PDPs without covering the whole processes consecutively and therefore, failed to provide detailed and integrated mechanisms of PDPs. In view of the insufficient information, low efficiency and the high cost of the present evaluation approaches, it was of great academic and industrial importance to develop a novel approach to investigate the PDPs of DPIs.

The modular process analysis platform (MPAP), developed in our previous research, demonstrated a potential to reach this goal. Previously, MPAP was applied to explore the influence of air flow rate during the PDPs[15]. The detailed mechanisms of air flow rate for PDPs of DPIs were successfully demonstrated, whose reliability was also preliminarily verified by NGI. This approach was competent to provide adequate and detailed information, with low

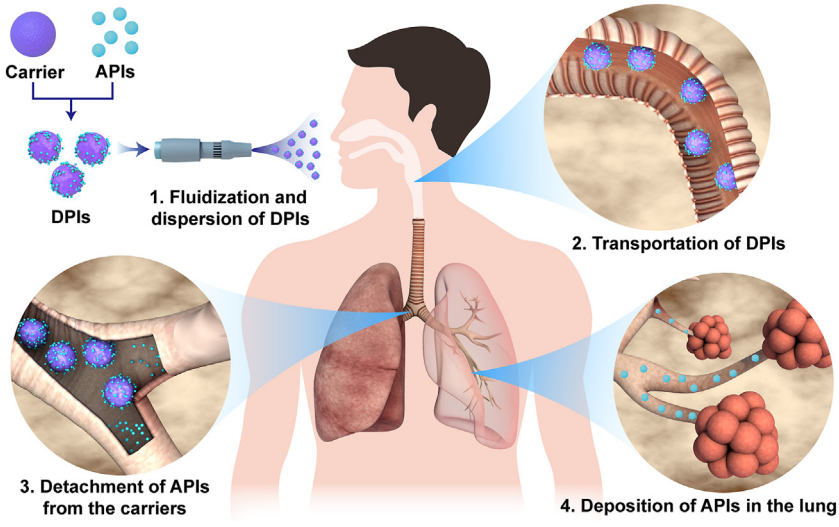

Figure 1 Schematic diagram of the pulmonary delivery processes of carrier-based DPIs.

cost and high efficiency. Specifically, it realized real-time monitoring of PDPs of DPIs in the inhaler device, throat and bronchi separately, which was the indispensable prerequisite for efficient optimization of DPIs. Except for the air flow rate, there were some other key factors that influenced the PDPs such as the physicochemical properties of carriers[16–18] and parameters of inhaler devices[19]. It was noteworthy that carriers served as the fundamental component of carrier-based DPIs due to their high proportions in the formulations[20]. Slight changes in the physical properties of carriers had enormous impacts on the PDPs. Among those properties, carrier particle size (CPS) was one of the most important factors, and was relatively easy to adjust in actual DPIs manufacturing to satisfy various formulation compositions[21].

CPS exercised great influence on PDPs of DPIs. The gravitational force (F_G) and inertia of carrier varied with different CPS, which would lead to premature deposition of DPIs in the inhaler device or throat to different extents. Besides, the numbers of active sites on the particle surface and surface roughness of carriers associated with the CPS, which directly altered the interparticulate force (F_I) between carrier−carrier and carrier–APIs. Thus, they affected the dispersibility of the particles, the following carrier detachment and drug delivery efficiency. Some researchers suggested that the FPF increased with smaller carrier particle size due to weaker adhesive force[21,22]. In contrast, others reported that improvement in aerosolization performance was observed with larger-sized carrier because of the superior dispersibility[23] and longer residence time[24]. Meanwhile, some studies demonstrated that the impact of CPS varied with the different shapes of carriers[25] or the different inhaler devices[26]. Despite of the importance of CPS, the detailed PDPs mechanism of DPIs with different CPS had not yet reported. As a matter of fact, the available studies proposed contradictory and inconclusive results. They might be caused by the different sieving methods of carrier, drug proportion or inhaler devices, which needed to be unified to investigate the effect of CPS.

In the present study, MPAP was applied to explore the effect of CPS and the mechanisms in the PDPs of DPIs. The reliability of MPAP was further demonstrated and its potential in optimizations of DPIs was studied. As shown in Fig. 2, MPAP was composed of a laser particle size analyzer (Fig. 2A, Sympatec HELOS, Sympatec GmbH, Clausthal-Zellerfeld, Germany), an inhaler device, an artificial throat and a pre-separator (Fig. 2B). The inhaler device was employed to assess the fluidization and dispersion processes of DPIs. The transportation of DPIs in the bended structure of human throat was mimicked by the artificial throat, which changed the orientation of air flow. Moreover, the bronchi bifurcation was simulated by the pre-separator, where the detachment mainly happened. Using real formulations in the MPAP test guaranteed the obtained results of physical properties of carriers or drugs were not simplified. Meanwhile, the release profiles of drug, drug aggregation and carrier could be monitored in real-time by the time-sliced measurement of MPAP, so that the function of each component in PDPs could be investigated. Notably, high efficiency and low cost of PDPs measurement were achieved by MPAP with quick detection (about 1 min) and small amount of sample (as low as 10 mg), which was beneficial for preliminary optimizations and quality control of DPIs manufacturing. In addition, Freeman Technology 4 (FT4) Powder Rheometer (Freeman Technology, Tewkesbury, UK) and NGI were employed to explore the powder flow properties of carriers and the aerosolization performance of DPIs respectively, which served as a reference to interpret and verify the results of MPAP. A good linear relationship was established between the results of NGI and MPAP, which confirmed the reliability and feasibility of MPAP for DPIs design and optimization.

2. Materials and methods

2.1. Materials

Lactose (LAC) including Inhalac® 251, Inhalac® 230 and Inhalac® 120 were generously donated by Meggle Pharma Co., Ltd. (Wasserburg, Germany). Salbutamol sulfate was obtained from Bidepharmatech Co., Ltd. (Shanghai, China). Hydroxy propyl methyl cellulose (HPMC) capsules 3# Vcaps® were generously donated by CAPSUGEL Co., Ltd. (Suzhou, China). Acetonitrile (analytically pure grade) was obtained from Saen Chemical Technology Co., Ltd. (Shanghai, China). Methanol (analytically pure grade) was obtained from Honeywell Burdick & Jackson, Inc. (Morris, NJ, USA). Monopotassium phosphate was supplied by Damao Chemical Reagent Factory Co., Ltd. (Tianjin, China).

2.2. Preparation of model DPIs

2.2.1. Micronization of salbutamol sulfate

Salbutamol sulfate was jet-milled by J-20 (TECNOLOGIA MECCANICA, Italy) with 6 kPa ring pressure and 7 kPa venturi pressure. Micronized salbutamol sulfate (MSS) was obtained and chosen as the model drug in the present study.

2.2.2. Sieving of lactose carrier

The commonly used inhalation lactose Inhalac 251, 230 and 120 were chosen to produce carriers of DPIs. They were produced from the same batch of lactose by sieving, which avoided the effect of different technological parameters. In the present study, they were sieved to obtain LAC with different particle size fractions (PSF). The targeted PSF, raw material and mesh size of sieve was presented in Table 1. They were placed on a mesh (200 μm) on mechanical shaker (AS200, RETSCH, Haan, Germany) and shaken for 2 min. Powder remained on the top of each different

Figure 2 Schematic diagrams of MPAP (A) Laser particle size analyzer; (B) Changeable module.

sieve (150, 100, 75 and 45 μm) was further subjected to air jet sieving (HOSOKAWA Micron Powder Systems, New Jersey, USA)) for 2 min to remove fine powder. When the sieving process was completed, LAC with different PSF was obtained.

2.2.3. Particle size distribution

The particle size distribution of MSS and LAC1–4 was measured by Sympatec HELOS&INHALER (Sympatec Gmbh, Clausthal-Zellerfeld, Germany). A single dose inhaler device Turbospin® (PH&T S.p.A., Milan, Italy) was used for dispersion and inserted into the adapter of INHALER. Start of the measurements was triggered by an optical concentration (C.OPT) larger than 0.3% and stopped at C.OPT smaller than 0.1%. The measurements were performed under air flow rate (U_0) of 60 L/min. R2 lens with a measurable particle size range of 0.25/0.45−87.5 μm and R4 lens with a measurable particle size range of 0.5/1.8−350 μm were chosen to detect the particle size distribution of MSS and LAC1–4, respectively. Meanwhile, the WINDOX software was used to control the measurement and analyze the results with the high-resolution Fraunhofer model. Three repeat measurements were conducted for each sample.

2.2.4. Preparation of model DPIs

The model DPIs were fabricated by blending MSS and LAC1–4 at a ratio of 1:15 (*w*/*w*) respectively, which were termed as DPI_1, DPI_2, DPI_3 and DPI_4. A Turbula T2F mixer (Glen Creston Ltd., Middlesex, UK) was applied for blending at 46 rpm for 60 min. The obtained model DPIs were packed into $3^{\#}$Vcaps® capsules with 10 ± 0.5 mg. The homogeneity of each model DPIs was evaluated (Supporting Information Section 1).

2.3. Surface roughness and morphology

A ContourGT Optical Profiler (Bruker Optics Inc., Billerica, USA) was used to measure the degree of surface roughness of LAC. Magnification lens (5 × , interferometry) with back scan equaled to 20 μm and the length of scanning equaled to 20 μs. The scanning area was 46.90 μm × 62.53 μm for all LAC samples. The average roughness (R_a), maximum profile valley depth (R_v) and maximum profile peak height (R_p) were obtained.

The morphology and chemical element distribution of MSS, LAC and model DPIs were examined by Gemini 500 scanning electron microscope (SEM, Bruker Optics Inc., Billerica, USA) equipped with energy-dispersive X-ray spectroscopy (EDXS). Samples were placed on aluminum stubs prior to imaging. The SEM and EDXS images were captured at an acceleration voltage of 3.0 and 6.0 kV, respectively. Oxygen (O) spectra and sulfur (S) spectra images were captured by EDXS, which represented LAC ($C_{12}H_{22}O_{11}$) and MSS [$(C_{13}H_{21}NO_3)_2 \cdot H_2SO_4$], respectively.

2.4. Powder flow properties measurement

The powder flow properties of LAC were characterized by FT4 Powder Rheometer (Freeman Technology). The standard dynamic test, aeration test and permeability test were conducted, and a conditioning cycle that removed the packing history and operator differences was performed before all the tests. The detailed method of FT4 was presented in Supporting Information Section 2. All the measurements were performed in triplicate.

2.5. The effect of CPS on pulmonary delivery processes of DPIs: MPAP

Three different configurations of *MPAP* were set up to explore the PDPs of DPIs with various CPS in inhaler device (Fig. 3A), artificial throat (Fig. 3B) and pre-separator (Fig. 3C). The single dose Turbospin® was selected as model inhaler device. The inhaler resistance of Turbospin® was 59.8 L/min when P_1 of NGI was set to 4.0 kPa as the pressure of human lung. The measurements were conducted under the U_0 of 60 L/min with the following parameters. Start and stop of the measurements was triggered on a C.OPT of 1.0% and 1.0%, respectively. A R4 lens was applied to the measurements and the duration was 4 s. The data were recorded in 100 ms sections with a 50 ms time base. Each sample was quantified in triplicate. WINDOX 5.0 software was used for data analysis. The involved parameters were descripted in Supporting Information Section 3. The product of C.OPT and dQ_3 was defined as release amount (R) of particles, which was recorded in each 100 ms. Release profile was plotted by time (T) as X-axis and R as Y-axis, and points were connected by smooth curves. The area under the curve of release profile was integrated by Origin 8.5 Software (Origin Lab, Northampton, MA, USA), which was defined as R_{AUC}.

2.6. In vitro aerosolization performance: NGI

The *in vitro* aerosolization performance of model DPIs was evaluated by NGI. Turbospin® and Tween® 80 (1% in ethanol, *v*/*v*) were selected as the inhaler device and surface coating of NGI stages. A batch of 20 capsules of each model DPIs were shot in each run under air flow rate of 60 L/min for 4 s. Ultra-pure water was used to collect MSS and LAC deposition on the inhaler device, adaptor, induction port, pre-separator, all NGI stages and micro orifice collector (MOC). The deposition profile of MSS and LAC was obtained by high performance liquid chromatography (HPLC) quantification[15]. The experiments were conducted in triplicates. The FPF values were calculated by CITDAS® software (version 3.10, Copley Scientific Ltd., Nottingham, UK).

Table 1 Sieving of lactose carrier.

Formulation	Targeted PSF (μm)	Raw material	Mesh size for air jet sieving (μm)	Mesh size for mechanical shaker (μm)
–	–	–	–	45
LAC1	45−75	Inhalac 251	45	75
LAC2	75−100	Inhalac 230	75	100
LAC3	100−150	Inhalac 120	100	150
LAC4	150−200	Inhalac 120	150	200

–Not applicable; PSF, particle size fraction; LAC, lactose.

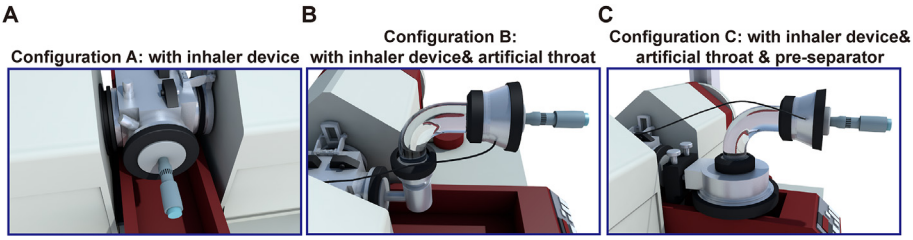

Figure 3 Schematic illustration of (A) Configuration A: laser particle size analyzer with inhaler device; (B) Configuration B: laser particle size analyzer with inhaler device & artificial throat; (C) Configuration C: laser particle size analyzer with inhaler device & artificial throat & pre-separator.

Table 2 Particle size distribution of LAC and MSS.

Formulation	D_{10} (μm)	D_{50} (μm)	D_{90} (μm)	Span
MSS	1.15 ± 0.04	2.88 ± 0.10	7.72 ± 0.60	3.08 ± 0.12
LAC1	41.66 ± 0.14	65.97 ± 0.12	91.70 ± 1.55	2.02 ± 0.02
LAC2	67.33 ± 1.15	99.87 ± 0.27	132.92 ± 0.41	2.01 ± 0.01
LAC3	86.31 ± 0.66	124.33 ± 0.35	160.11 ± 0.30	1.98 ± 0.01
LAC4	98.96 ± 2.23	152.30 ± 0.50	194.17 ± 0.47	1.92 ± 0.02

All data were presented as mean ± SD, $n = 3$. LAC, lactose; MSS, micronized salbutamol sulfate.

2.7. *Statistics analysis*

All the data were showed as mean ± standard deviation (SD), if possible. SPSS Statistics V 17.0 software (IBM Corporation, Armonk, NY) was employed for statistical analysis. One-way analysis of variance (ANOVA) and unpaired two-sample *t*-test were used to data analysis. *P* value higher than 0.05 was determined as statistically significance. Besides, R^2 value higher than 0.9 suggested a strong correlation.

3. Results and discussion

3.1. *Particle size distribution*

Particle size distributions of LAC and MSS are shown in Table 2. The D_{50} values of MSS are smaller than 5 μm, indicating the suitability of the MSS in pulmonary drug delivery. Moreover, particle size distributions of LAC were far larger than MSS and not overlapping. It suggested that LAC and MSS could be distinguished by MPAP and were able to be used in the following studies.

The D_{10}–D_{90} of MSS and LAC obtained from Sympatec HELOS&INHALER served as a reference of the primary size of drug and carrier. Particles with the size range from D_{90} of MSS to D_{10} of LAC were defined as drug aggregation. The results are present in Table 3.

Table 3 The primary particle size of drug, drug aggregation and carrier.

Formulation	Primary particle size (μm)
MSS	1.15−7.72
LAC1	41.66−91.70
Drug aggregation-1	7.72−41.66
LAC2	67.33−132.92
Drug aggregation-2	7.72−67.33
LAC3	86.31−160.11
Drug aggregation-3	7.72−86.31
LAC4	98.96−194.17
Drug aggregation-4	7.72−98.96

LAC, lactose; MSS, micronized salbutamol sulfate.

3.2. *Surface roughness and morphology*

The 3D images of LAC surfaces acquired by optical profiler are presented in Fig. 4A and the corresponding R_a values are shown in Fig. 4B. The surface of LAC1 was covered by serried and uniform projections with a few deep voids, which possessed the lowest R_a among all LAC samples. With the increase of particle size, some scattered large peaks appeared on the LAC2 surface, while majority of the surface was still covered with dense and small projections. The number of large peaks kept increasing in LAC3 and their distribution tended to be even. Meanwhile, there were many deep voids (blue color) appeared in LAC3, suggesting the increased roughness of surface and thus increased R_a. Furthermore, the highest density of large peaks showed up on the surface of LAC4, which resulted in the highest value of R_a. In summary, the density of large peaks on the surface increased with the increased particle size of LAC, and the R_a values presented the same tendency. The SEM images of LAC (Supporting Information Section 4) demonstrate the same results that the surface roughness (*e.g.*, granular structures and local projections) increased with larger LAC particle size.

The EDXS images of LAC, MSS and DPI_1–DPI_4 are presented in Fig. 4D and E. Fig. 4Da and 4Dc are the optical images of MSS and LAC, respectively, which served as the comparisons of their S and O spectra images. The yellow and purple colors represent S atoms of MSS (Fig. 4Db) and O atoms of LAC (Fig. 4Dd), respectively. The merged images of DPIs (Fig. 4E) show that drug particles (yellow color) were evenly distributed on the carrier surface (purple color) of DPI_1 and DPI_2, while some drug particles scattered. Besides, when the CPS of DPIs increased as well as R_a, drug particles tended to mainly distribute in the deep voids of carrier. Moreover, the results of EDXS are also exemplified by the SEM images of DPIs (Supporting Information Section 4).

Some studies[27−30] have confirmed that the R_a of carrier was relevant to the adhesive force between carrier and drug in carrier-based DPIs, which affected the detachment process in the

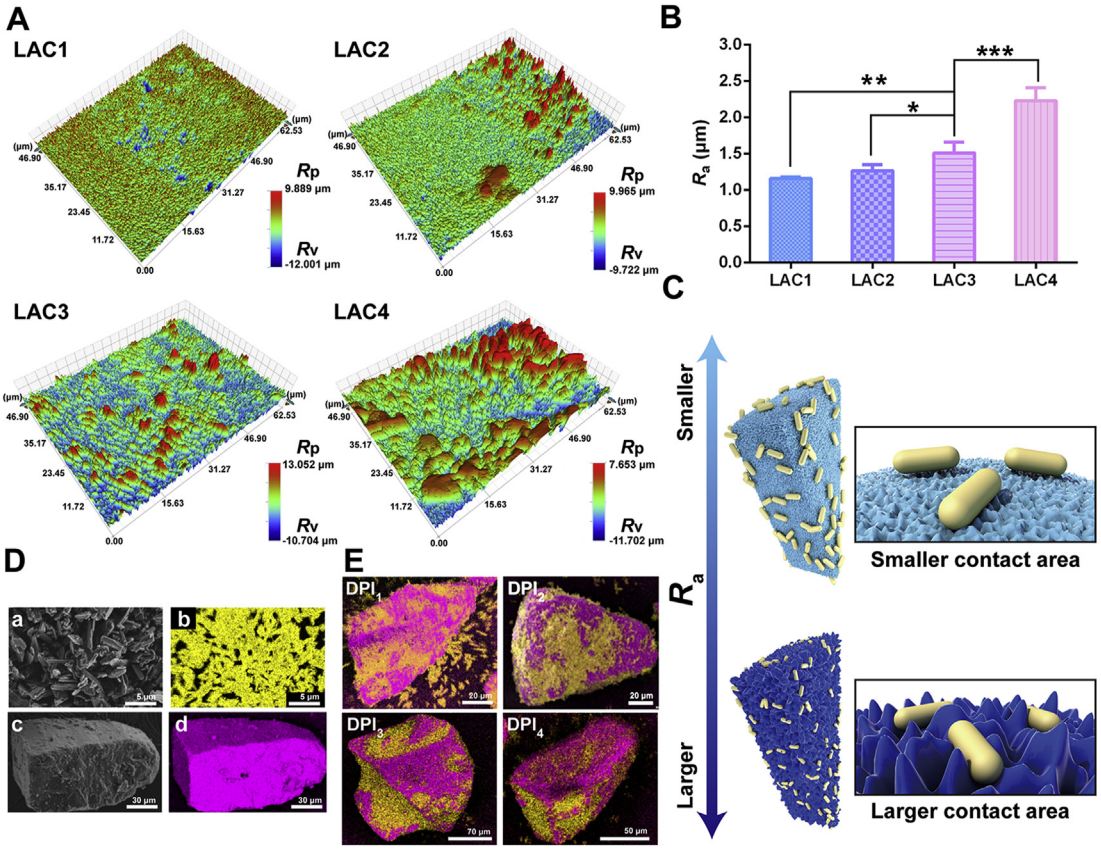

Figure 4 (A) 3D images of LAC surfaces; (B) R_a of LAC surfaces; (C) Schematic diagram of LAC with different R_a; (D) SEM images of (a) MSS and (c) LAC. EDXS images of (b) MSS and (d) LAC; (E) EDXS images of DPI_1–DPI_4 (All data were presented as mean ± SD, $^*P < 0.05$, $^{**}P < 0.01$, $^{***}P < 0.005$, $n = 3$).

pulmonary delivery. The R_a value had a great impact on the interaction between carrier and drug. The larger R_a led to higher adhesive force due to larger contact area, which was defined as the active sites[31,32]. Due to the serried and uniform projections on LAC1 and most part of LAC2 surface, the degree of surface discontinuities was too small to allow the drug particles to insert into the tiny cavities on the surface and consequently, the contact area between drug and carrier and the corresponding adhesive force were small (Fig. 4C). On the contrary, the projections on the carrier surface became larger and taller when particle size increased, forming big cavities on the surface. In this case, drug particles could easily imbed into the cavities and adhere to the carrier by mechanical interlocking. Meanwhile, the contact area between drug and carrier became larger, resulting in the increase of the Van der Waals force and the Coulomb force, which might intensify the interaction between drug and carrier but also, hinder the detachment of drug and carrier (Fig. 4C). For LAC1–4, the results indicate that the carrier with smaller particle size had lower R_a, which would be beneficial to the detachment process in pulmonary delivery of DPIs.

3.3. *Powder flow properties*

The FT4 powder rheometer was used to investigate the powder flow properties of LAC. The TE, BFE and SE values obtained from dynamic tests are shown in Fig. 5A. The TE values were increased with the growth of LAC particle size, which served as an indicator of flow resistance (Fig. 5Aa)[33]. It revealed that LAC with smaller particle size showed lower resistance to air flow, representing superior flowability. When the particle size of LAC was larger, the mass of particles increased and the F_G acted on each particle was increased. Thus, the press-on force (F_P) acted on the under particles was greater as well. In addition, the R_a values climbed up with the increment of particle sizes, which indicating larger friction coefficients. Hence, the friction force (F_F) increased between particles of LAC with larger particle sizes as shown in Eq. (1):

$$F_F = \mu F_P \tag{1}$$

where μ represents the friction coefficient of the contact surface.

More energy was consumed to conquer the F_F between particles, when the blade moved through the powders (Fig. 5Ad and e). Therefore, the TE values increased along with larger particle size of LAC. LAC1 possessed the lowest TE and the best flowability, which suggested superior aerosolization performance. In the last three test cycles, the TE values of LAC2 increased slightly then remained stable, while LAC3–4 increased obviously then decreased to the level before. The tip speed of the blades was decreased in the last three test cycles, and higher TE was needed to move the blades for powder with higher R_a and inferior flowability. Since the tip speed in the last cycle was very low, particles had enough time to move behind the blades and the resistance to the front of the blades decreased. Thus, the TE values of LAC3–4 decreased in the last test cycle. Besides, there was no significant change of the TE values of LAC1, suggesting its good flowability. In contrast, LAC1 presented the upward trend of TE at smaller

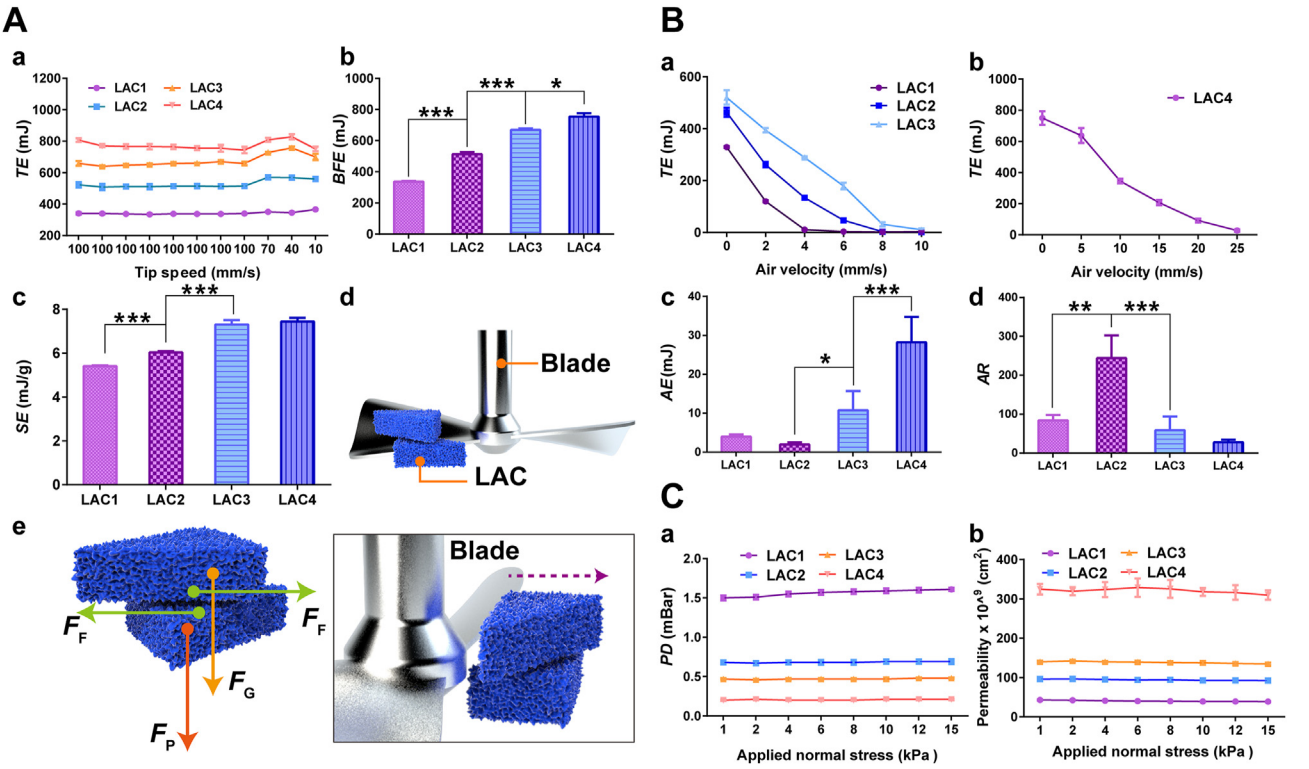

Figure 5 (A) Dynamic test results of LAC. (a) Total energy (TE) *vs.* dynamic profiles; (b) Basic flow energy (BFE); (c) Specific energy (SE); (d) Schematic diagram of blade and LAC during dynamic test; (e) Force analysis of LAC during dynamic test; (B) Aeration test results of LAC. (a) TE *vs.* aeration profiles of LAC1–3; (b) TE *vs.* aeration profiles of LAC4; (c) Aerated energy (AE); (d) Aeration ratio (AR); (C) Permeability test results of LAC. (a) Pressure drop (PD) across the powder bed *vs.* applied normal pressures of LAC; (b) Permeability *vs.* applied normal pressures of LAC (All data were presented as mean ± SD, $*P < 0.05$, $**P < 0.01$, $***P < 0.005$, $n = 3$).

blade speed (10 mm/s) and the change of the TE values of LAC1 was slight, suggesting its good flowability.

The BFE values increased as the LAC of larger particle sizes were used in the test (Fig. 5Ab), which indicated the deterioration of flowability and verified the results from the TE values. In addition, the SE values increased from LAC1 to LAC3, while there was no obvious difference between LAC3 and LAC4 (Fig. 5Ac). Higher SE values suggested stronger total F_I in each gram of powder[33]. LAC1 had the lowest SE values, which was beneficial to the detachment of carrier and drug during pulmonary delivery. Besides, each particle of LAC3 possessed smaller R_a and mass than LAC4, which resulted in smaller F_I between two particles. However, it was counterbalanced and surpassed by the larger quantity of LAC3 particles under the same quality conditions, due to its smaller particle size and density. Thus, the SE values of LAC3 and LAC4 were similar.

The TE, AE and AR values acquired from aeration test are presented in Fig. 5B. The aeration test was employed to evaluate the decrement of flow energy when air flow was introduced. It was applied to depict the powder behavior of DPIs during blending process, fluidization and transportation processes, which was of significance for pulmonary delivery efficiency[5,33]. The TE of LAC1 and LAC2 became stable when air velocity reached four and 8 mm/s, respectively (Fig. 5Ba). The stable state of TE indicated fully fluidization of powder and minimum air velocity that reached fluidized state (minimum fluidize velocity, MFV)[34]. Lower MFV of LAC1 suggested that it was easier to be fluidized and delivered into deep lung. In addition, the TE values of LAC3 and LAC4 barely reached stable at 10 and 25 mm/s, respectively, demonstrating they were harder to be fluidized compared with LAC1–2 (Fig. 5a and b). It may be due to the larger F_G and F_I of LAC3–4 led to prematurely deposition during pulmonary delivery processes. Furthermore, the higher AE and AR values meant the powder were more cohesive and more sensitive to air flow, respectively[35,36]. LAC1 and LAC2 both possessed low AE values, showing their small cohesive force during aeration (Fig. 5Bc). Meanwhile, the AE values of LAC1 were slightly higher than that of LAC2, which might result from higher Coulomb force in LAC1. LAC1 possessed smaller particle size than LAC2, indicating that the voids between particles in LAC1 were also smaller. When aerated, particle friction generated static electricity and the Coulomb force that reduced the distance between particles. A little extra energy was needed to be surmounted when LAC1 aerated. However, the effect of Coulomb force decreased with the increasing of particle size. Therefore, the AE values of LAC1 were slightly higher than that of LAC2. LAC4 had the highest AE values, suggesting the largest cohesive force of LAC4. Moreover, the AR values of LAC2 are much higher than that of other LAC samples (Fig. 5Bd). The results showed that the balance of particle size, Coulomb force and R_a ensured the superior sensitivity of LAC2 to air flow.

The PD and permeability values obtained by permeability test are shown in Fig. 5C. Permeability test was used to measure the ease of air flow passed through powder under various pressures[37]. The lower PD values suggested higher permeability, which were beneficial for better dispersion, fluidization and transportation of DPIs[38]. The PD values of all LAC samples were small and almost remained stable when applied normal stress increased, showing

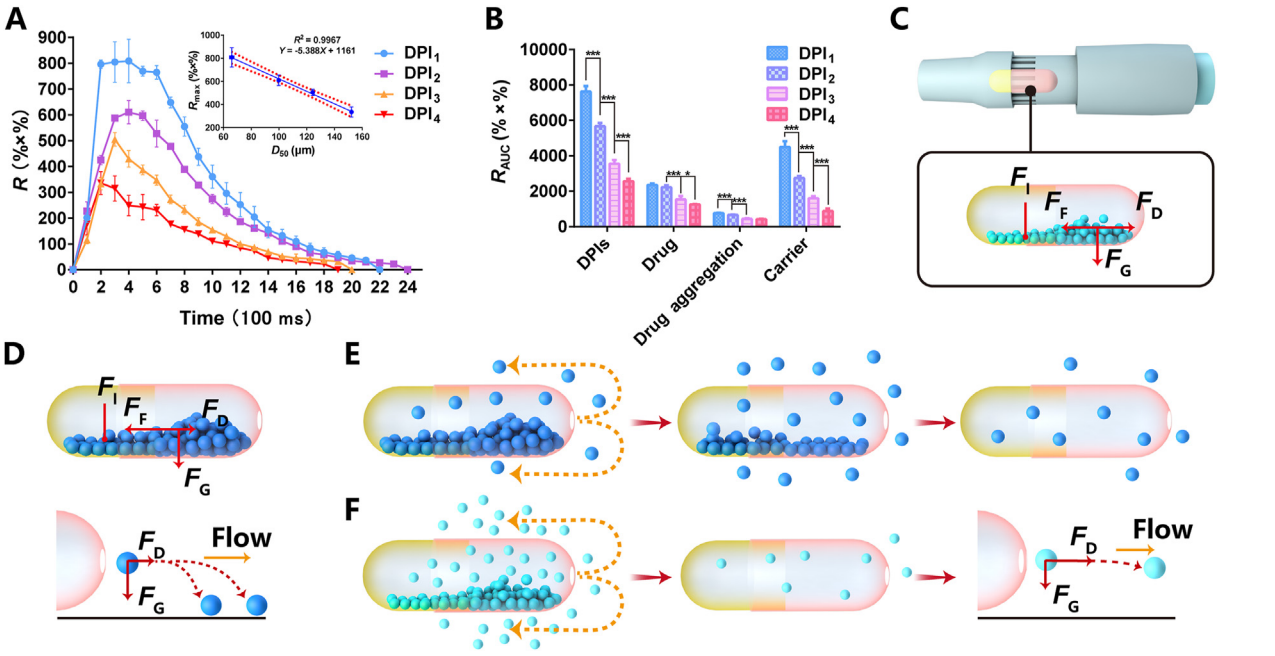

Figure 6 Configuration A (A) Release profiles of DPIs. Inset was the correlation between D_{50} of LAC and R_{max}; (B) Total release amount; (C) Force analysis of DPIs in the capsule within inhaler device; (D) DPIs with larger CPS remained in the capsule or deposited prematurely; (E) The release of DPIs with larger CPS; (F) The release of DPIs with smaller CPS (all data were presented as mean ± SD, $^{*}P < 0.05$, $^{**}P < 0.01$, $^{***}P < 0.005$, $n = 3$).

good permeability of LAC (Fig. 5Ca). The PD values decreased and the permeability increased when the particle size increased (Fig. 5Cb). This could be explained as that the voids between particles increased with the increment of particle size, which was easier for the air flow to pass through and showed higher permeability.

3.4. The effect of CPS on pulmonary delivery processes of DPIs: MPAP

Carrier served as a fundamental component in carrier-based DPIs due to its high proportion. Hence, the physicochemical properties of carrier had an essential influence on aerosolization performance of DPIs. Carriers with different particle size possessed various inertia and drug payload, and were subjected to different degrees of F_D, F_G and F_I which greatly affected the PDPs and pulmonary drug delivery efficiency. Therefore, MPAP was employed to explore the effect of CPS on PDPs with a model DPIs. To be specific, the fluidization and dispersion of DPIs in inhaler device, the transportation, detachment and deposition in artificial throat and pre-separator were investigated in detail. In addition, the mechanism of carrier particle size on each PDP was explored.

3.4.1. Configuration A: With inhaler device

Primarily, the inhaler device was equipped on the laser particle size analyzer to obtain configuration A (Fig. 3A). The PDP of DPIs in inhaler device was expounded with the real-time release profile of drug, drug aggregation and carrier. In addition, the R_{AUC} served as an indicator to show the detachment and deposition of DPIs. Thus, the impact of CPS on the fluidization, dispersion and premature deposition of DPIs in the inhaler device was explored.

The release profiles of DPIs with different CPS are presented in Fig. 6A. The R values increased in the first place and decreased subsequently, which was similar to the breath of human. The R_{max} (Fig. 6A) and R_{AUC} (Fig. 6B) of DPIs increased along with the decrease of CPS. DPI_1 exhibited the highest R_{max}, which was 1.43-, 1.60-, and 2.41-fold of DPI_2, DPI_3 and DPI_4, respectively. Meanwhile, the R_{AUC} of DPI_1 was much higher than that of DPI_4 (2.98-fold). Good linear relationships between R_{max} and D_{50} of corresponding LAC ($R^2 = 0.9967$) as well as R_{AUC} and D_{50} of corresponding LAC ($R^2 = 0.9802$) were established, respectively.

The DPIs particles were subjected to many forces when being released from the capsule, which primarily consisted of the drag force of air flow [F_D, Eq.(2)][39,40], F_G [Eq.(3)][41], F_I[42,43] and F_F[44] between particle−particle and particle-capsule wall (Fig. 6C).

$$F_D = 3\pi\eta X d U_0 / C_C \tag{2}$$

$$F_G = mg = \rho V g = \rho g \pi d^3 / 6 \tag{3}$$

where η represents the viscosity of the air, X denotes the dynamic shape factor, d represents the diameter of particle, C_C is the Cunningham correction factor for slip flow, ρ represents the bulk density, m represents the mass of particle and V is the volume of particle.

Of note, F_D and F_G dominated the release process of particles from the inhaler device[45]. According to Eqs. (2) and (3), F_G was more influenced by particle diameter (d) than F_D, since F_G was proportional to the third power of d. When CPS increased, F_G of DPIs particles increased drastically. Meanwhile, higher R_a also led to larger F_F. It was relatively hard for larger DPIs particles to be entrained by air flow. Instead, they tended to remain in the capsule, deposit early (Fig. 6D) or release slowly from the capsule to reach the detector (Fig. 6E), resulting in low R_{max} and R_{AUC} values. The results revealed that DPIs with larger CPS were prone to deposit on oropharynx and could not travel further for deeper drug delivery.

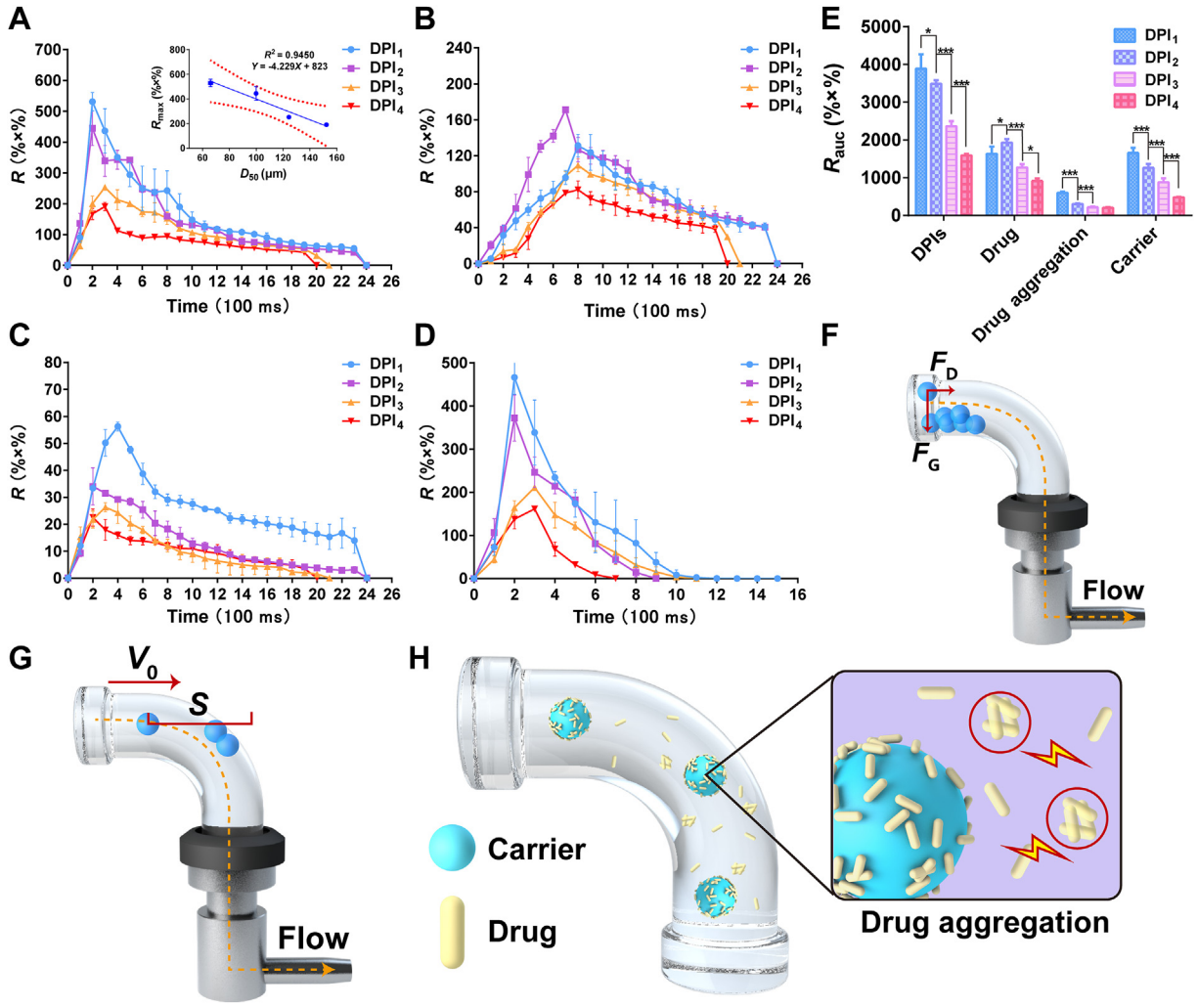

Figure 7 Configuration B (A) Release profiles of DPIs. Inset was the correlation between D_{50} of LAC and R_{max}; (B) Release profiles of Drug; (C) Release profiles of drug aggregation; (D) Release profiles of carrier; (E) Total release amount; (F) DPIs deposited before the corner of artificial throat; (G) The stopping distance of DPIs with larger CPS was longer than the distance between particle and the wall of artificial throat; (H) Drug aggregation was formed during transportation in artificial throat due to stronger impaction and Coulomb force (all data were presented as mean ± SD, $*P < 0.05$, $**P < 0.01$, $***P < 0.005$, $n = 3$).

In comparison, DPIs with smaller CPS were subjected to lower F_G and R_a, which allowed them easier to be fluidized, dispersed and released from the capsule to successfully reach the detector (Fig. 6F). The increased R_{max} and R_{AUC} of the DPIs with smaller CPS enabled the particles to be delivered into lower respiratory tract. Furthermore, the tendencies of R_{max} and R_{AUC} of DPIs confirmed the results of TE (Fig. 5Aa) and MFV (Fig. 5Ba and b), suggesting that LAC with smaller particle size had less resistance to air flow and was easier to fluidize. Moreover, the release profile of carrier was similar to that of DPIs, indicating weak detachment between drug/drug aggregation and carrier within inhaler device (Supporting Information Section 5). Regarding to drug and drug aggregation, R_{max} and R_{AUC} also increased with the smaller CPS and the detailed results were presented in Supporting Information Section 5.

In short, the fluidization and dispersion processes of DPIs with different CPS were monitored by configuration A. The release profiles showed that DPIs with smaller CPS were easier to be fluidized and released from the capsule when inhaled. It showed that DPIs with smaller CPS were prone to be transported into deeper airway instead of premature deposition. Meanwhile, the detachment between drug/drug aggregation and carrier increased with smaller CPS due to lower R_a and fewer active sites of smaller size carrier that reduced drug adhesion, and more severe impaction that promoted detachment. Thus, smaller CPS was considered more suitable for further transportation, but its possible adverse effect also needed to be considered owing to higher drug detachment.

3.4.2. Configuration B: With inhaler device & artificial throat

Configuration B was achieved by using the inhaler device and the artificial throat connected to the laser particle size analyzer by a customized connector (Fig. 3B), which was employed to explore the effect of throat on the transportation and detachment processes of DPIs.

Comparing to configuration A, all R_{max} and R_{AUC} of release profiles obtained by configuration B obviously declined, mainly due to the direction change of air flow caused by artificial throat. The release profiles obtained by configuration B were shown in Fig. 8. T_t, R_{max} (Fig. 7A and D) and R_{AUC} (Fig. 7E) of DPIs and

carrier increased with smaller CPS. Specifically, R_{max} of DPI_1 was 1.19-, 2.10- and 2.78-fold of that of DPI_2, DPI_3 and DPI_4, respectively. A linear correlation ($R^2 = 0.9450$) between R_{max} of DPIs and D_{50} of the corresponding LAC was observed. Notably, R_{AUC} of DPI_1 was 2.45-fold of that of DPI_4.

When the CPS increased, the F_G of DPIs increased consequently. Large F_G and inadequate F_D might give rise to deposition of DPIs particles on artificial throat rather than further transportation (Fig. 7F). Importantly, once DPIs particles reached the bend of artificial throat, they still had a velocity (V_0) towards the original orientation that kept particles moving forward. The required distance for reducing V_0 to zero was referred as stopping distance [S, Eq.(4)][46].

$$S = d^2 \rho U_0 C_C / 18 \eta X \quad (4)$$

where η is the viscosity of the air, X represents the dynamic shape factor, d denotes the diameter of particle, ρ is the bulk density and C_C represents the Cunningham correction factor for slip flow.

Inertial impaction and particle capture might take place when S was longer than the distance between the particles and the wall of artificial throat. According to Eq. (4), S was proportional to the second power of d, indicating that particles with larger size needed a longer stop distance and were more likely to collide with the wall of artificial throat and be captured, leading to less drug to reach the lung (Fig. 7G). Thus, R_{max} and R_{AUC} of DPIs and carrier decreased with larger CPS.

Regarding to the release profiles of drug, DPI_2 possessed the highest R_{max} (Fig. 7B). R_{AUC} of DPI_1 was 1.29- and 1.79-fold of that of DPI_3 and DPI_4, respectively, while DPI_2 was slightly higher than DPI_1 (Fig. 7E). Besides, R_{max} and R_{AUC} of drug aggregation decreased with increased CPS (Fig. 7C and E).

As previously mentioned, R_{AUC} of DPIs increased with smaller CPS and hence the detachment of drug and drug aggregation increased due to the lower R_a of carrier and fewer active sites as well as stronger impaction between particles. Meanwhile, when DPIs particles entrained by air flow and entered artificial throat, they were in a fully fluidized state. The EDXS images and AE, AR values obtained in aeration test could be applied to analyze the above results. For DPI_1, larger proportion of drug particles did not adhere to the active sites on carrier surface (Fig. 4E). Moreover, its smaller CPS resulted in greater chance of impaction, which generated more static electricity[47] and showed higher AE values

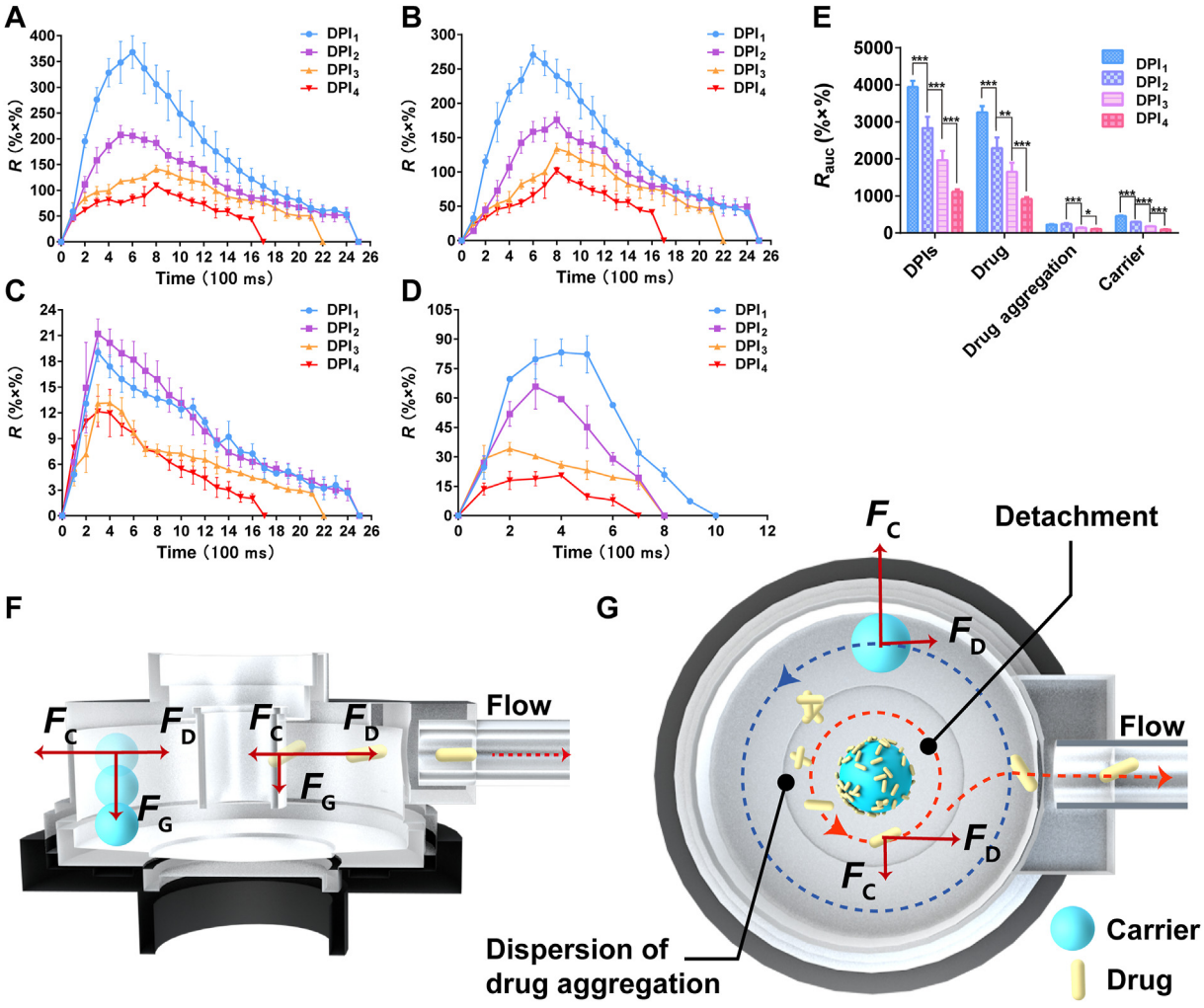

Figure 8 Configuration C (A) Release profiles of DPIs; (B) Release profiles of drug; (C) Release profiles of drug aggregation; (D) Release profiles of carrier; (E) Total release amount; (F) Carrier tended to deposit on pre-separator while drug could be further entrained by airflow; (G) Detachment of carrier–drug/drug aggregation and dispersion of drug aggregation due to different F_C (All data were presented as mean ± SD, $^*P < 0.05$, $^{**}P < 0.01$, $^{***}P < 0.005$, $n = 3$).

and lower AR values. As a result, drug particles in DPI_1 were easier to form drug aggregation due to stronger impaction and Coulomb force (Fig. 7H). In contrast, carrier of DPI_2 possessed larger R_a and more active sites. Smaller drug aggregations were formed during blending process compared to DPI_1, which were easier to be dispersed into drug particles. Meanwhile, less static electricity was generated for dispersed drug particles to reform aggregation in larger CPS. Hence, R_{AUC} of drug in DPI_2 was higher than that of DPI_1 while R_{AUC} of drug aggregation in DPI_2 was lower. However, the detachment of drug from carrier within throat was not beneficial to high pulmonary drug delivery efficiency.

It was well-known that when the detached drug particles released from throat in the human body, they would enter the long and moist trachea[48]. Due to the stronger electrostatic force and poorer flowability of fine particles, the drug particles detached in inhaler device or throat were more likely to adhere to the wall of trachea[49] and had smaller chance to travel into the lower parts of airways.

Besides, the internal geometry was more complex than artificial throat in real human body and moist mucus layers also existed, which might lead to more particle deposition without bouncing back. Thus, the Alberta throat[50] with more detailed internal geometry and 1% Tween® 80[9] could be applied in the future study for acquiring more realistic correlation between *in vitro* simulation and *in vivo*.

In summary, configuration B of MPAP was demonstrated useful in the investigation of DPIs transportation and detachment. Since the deposition of DPIs particles before the bend of artificial throat and inertial impaction with the wall of artificial throat hindered the further transportation of DPIs, R_{AUC} of DPIs were obviously lower than those in Configuration A. Besides, the release profiles and R_{AUC} showed that the detachment of drug and drug aggregation from carriers became more distinct while CPS was smaller, since the lower R_a, fewer active sites of carrier and stronger impaction between particles−particles. However, the prematurely detached drug particles from carrier within the inhaler device or artificial throat endowed a great chance to be captured before reaching deep lung, which was not desirable for pulmonary drug delivery.

3.4.3. *Configuration C: With inhaler device & artificial throat & pre-separator*

Configuration C was obtained by using the inhaler device, the artificial throat and the pre-separator equipped to the laser particle size analyzer (Fig. 3C). Pre-separator was introduced to investigate the detachment process of DPIs in the bronchi bifurcation of human.

Compared with configuration B, the R_{max} and R_{AUC} of drug (Fig. 8B and E) significantly increased, while those of drug aggregation (Fig. 8C and E) and carrier (Fig. 8D and E) decreased in configuration C. DPIs particles were under the influence of centrifuge force (F_C) besides F_D and F_G, when entered the pre-separator. According to Eq. (5), F_C was proportional to the third power of d, which indicated a significant impact of d on F_C[46].

$$F_C = mU_0^2/r = \pi d^3 U_0^2/6r \quad (5)$$

where m is the mass of particle, r represents the radius of centrifugal motion, d denotes the diameter of particle.

Since there were great differences between d of drug or drug aggregation and carrier, the F_C of each subject varied. For carriers, they possessed larger particle size and bigger F_C, so their movements tended to be close to the wall of pre-separator, resulting in bigger potential to deposit. In contrast, drug and drug aggregation with smaller particle size were inclined to move near the center of pre-separator. Different F_C of these subjects generated the separation effect, which overcame the particle adhesion and promoted the drug detachment between drug aggregations or drug−carrier complex (Fig. 8G). Therefore, R_{AUC} of drug markedly increased while R_{AUC} of drug aggregation and carrier decreased.

The release profiles and R_{AUC} obtained by configuration C were presented in Fig. 8. The R_{max} and R_{AUC} of DPIs (Fig. 8A) increased for smaller CPS, which mainly due to the increased detachment of drug particles. Although increased CPS would theoretically benefit the detachment due to the greater difference of F_C, more active sites and higher R_a of larger CPS greatly restrained the drug detachment process. Besides, the larger specific surface area (SSA) of carrier with smaller particle size might result in more chance of adhesion and less detachment between drug and carrier. The R_{max} and R_{AUC} of drug (Fig. 8B and E) increased with smaller CPS, which proved that the quantity of active sites and R_a imposed greater influence than F_C and SSA on the detachment process. Although in configuration B, DPI_1 tended to form drug aggregations due to generated static electricity, the F_C acted on drug aggregation might overcome this cohesive force and re-disperse the drug particles within the pre-separator (Fig. 8G), which also led to the highest R_{max} and R_{AUC} of drug in DPI_1. The released drug particles within the pre-separator had greater chance to be efficiently transported into the lower parts of airways and deposited on the deep lung. The results showed that DPI_1 had better drug detachment property and implied that LAC1 was optimal for efficient pulmonary drug delivery due to its suitable particle size and surface roughness.

DPIs with larger CPS would suffer from greater F_G and consequently, lead to greater acceleration of downward movement (Fig. 8F), increased deposition on the bottom of the pre-separator and reduced time for drug detachment and eventually, lower R_{max} and R_{AUC} of carrier (Fig. 8D and E). On the contrary, the DPIs of smaller CPS (*e.g.*, DPI_1) had increased R_{max} and R_{AUC} and longer T_t of carrier, which proved to be able to facilitate further delivery of drug particles into deep lung.

In brief, the transportation and detachment processes within bronchi bifurcation of DPIs were mimicked by the configuration C. The detachment between drug and carrier in the pre-separator was more efficient than that in the artificial throat and inhaler device, due to the F_C generated by vortex air flow within the pre-separator. During this process, the detached drug particles had greater potential to be delivered into deep lung, while carriers tended to deposit due to larger F_G and F_C. Besides, the CPS played important role in the detachment of DPIs. The R_a and quantity of active site in different carriers dominated the detachment process. LAC1 with the smallest particle size among all carriers possessed the lowest R_a and the fewest active sites. It was beneficial for detachment of drug and carrier, and thus became the optimal CPS in the present study.

3.5. *In vitro aerosolization performance: NGI*

NGI, which was the globally recognized method for the evaluation of *in vitro* aerosolization performance of DPIs[12,51,52], was employed in the present study to explore the influence of CPS on

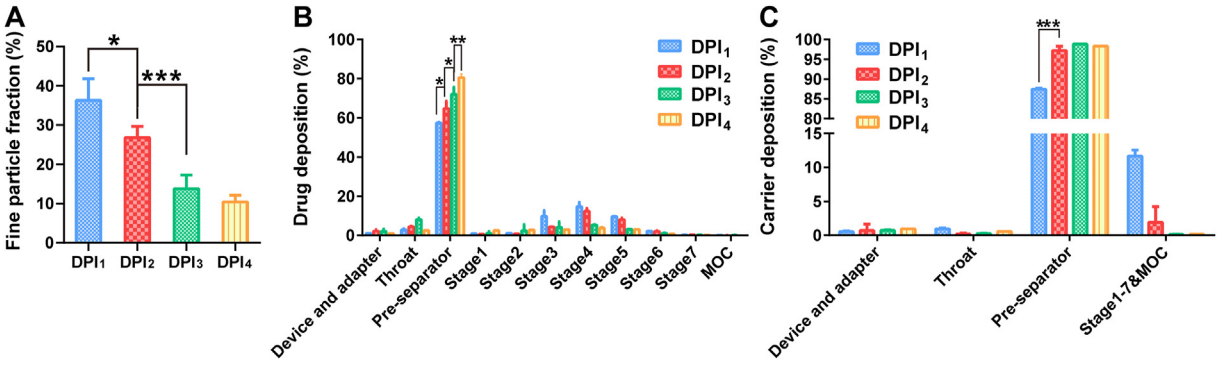

Figure 9 *In vitro* aerosolization performance of DPI_1–DPI_4 (A) The FPF values; (B) Drug deposition profile; (C) Carrier deposition profile (All data were presented as mean ± SD, $^*P < 0.05$, $^{**}P < 0.01$, $^{***}P < 0.005$, $n = 3$).

the PDPs of DPIs. Besides of the investigation on drug particles, the carrier deposition was also measured to further understand PDPs.

The result of drug recovery rate measured by NGI was presented in Supporting Information Section 6, which were larger than 85% and met the requirement of NGI test. The FPF values increased with the decrease of CPS. DPI_1 showed 3.49-fold FPF value to DPI_4 (Fig. 9A). Most drug particles deposited on the pre-separator and the deposition increased with the CPS (Fig. 9B). In regards to the carrier (Fig. 9C), more than 95% of particles of LAC2–4 deposited on the pre-separator and failed to reach lung. In contrast, a higher proportion (11.68 ± 0.89%) LAC1 entered the lower stages and facilitated deeper pulmonary drug delivery. It was obvious that DPI_1 with the smallest CPS showed optimal aerosolization performance.

Since the R_a and the quantity of active sites of carrier increased with the larger particle size, detachment of drug particles from the carrier was more difficult. Meanwhile, carriers with larger size were subjected to larger F_G, which led to greater possibility to deposit on the pre-separator. Hence, DPIs with smaller CPS were considered as the better system in the present study (*e.g.*, LAC1) for their superior efficiency for pulmonary drug delivery. A good linear relationship ($R^2 = 0.9557$) was established between the FPF and R_{AUC} of drug in configuration C. The results confirmed that the MPAP was a feasible approach to evaluate the mechanism of PDPs during DPIs development.

4. Conclusions

The main aim of this study was to apply MPAP to investigate the effect of CPS and the mechanisms in the PDPs of DPIs. As a key factor in PDPs, the CPS was considered to have great influence in the efficiency of pulmonary drug delivery greatly and was comprehensively investigated in the present study. The surface morphology and powder properties of carriers with different particle sizes were explored. Then, the MPAP was innovatively employed to mimic the PDPs of DPIs with different CPS in inhaler device, throat and tracheal bronchus, respectively. The results of the experiments revealed that the R_a, quantity of active site and F_G varied according to the different CPS, which led to different performance of PDPs. The R_{AUC} of DPI_1 was much higher than that of DPI_4 (2.98-fold) in configuration A. Besides, the R_{AUC} of drug in DPI_1 was 3.68-fold of DPI_4 in configuration C. According to the results of MPAP, DPIs with smaller CPS (*e.g.*, LAC1) tended to undergo easier fluidization and dispersion in the inhaler device. Although drug particles of DPIs with the smallest CPS tended to aggregate because of stronger static electricity, their lower R_a and smoother surface were beneficial for the detachment process of drug from the carrier in the pre-separator, which eventually led to better performance of pulmonary drug delivery. For the range of particle size in the present study (41.66−194.17 μm), the optimal applicable range of CPS of DPIs was 41.66−91.70 μm. However, the applicable range of CPS needed to be subdivided and expanded to obtain a more precise result, which could be applied in the manufacture of DPIs. In conclusion, this study confirmed that the physicochemical properties of carrier with various particle sizes were the key parameters to understand the mechanism of PDPs. Incorporating these factors into a real-time monitoring system such as MPAP would be highly feasible and promising to facilitate the development of DPIs.

Acknowledgments

This paper was funded by the Fundamental Research Funds for the Central Universities (Nos. 21620434 and 2162014, China), the National Natural Science Foundation of China (Nos. 81673375 and 81703431), the Science and Technology Foundation Guangzhou (No. 201509030006, China) and the National Students Innovation Training Program of China (No.201901390, China). The authors thanked DSKH (Shanghai) Ltd. and Micromeritics Instrument (Shanghai) Ltd. for the technical support.

Author contributions

Yingtong Cui and Xuejuan Zhang designed the experiment, analyzed the data and wrote the manuscript. Yingtong Cui, Xiangyun Lu, Jun Xue, Guanlin Wang, Xiao Yue and Ziyu Zhao helped to perform the experiments. Ying Huang, Xuejuan Zhang and Ping Hu revised the manuscript and the artworks. Ying Huang, Xin Pan and Chuanbin Wu were responsible for fund-seeking, supervision and proof-reading. All of the authors have read and approved the final manuscript.

Conflicts of interest

The authors have no conflicts of interest to declare.

Appendix A. Supporting information

Supporting data to this article can be found online at https://doi.org/10.1016/j.apsb.2021.06.011.

References

1. Yu SH, Yuan HY, Chai GH, Peng K, Zou PZ, Li XX, et al. Optimization of inhalable liposomal powder formulations and evaluation of their *in vitro* drug delivery behavior in Calu-3 human lung epithelial cells. *Int J Pharm* 2020;**586**:119570.
2. de Boer AH, Hagedoorn P, Hoppentocht M, Buttini F, Grasmeijer F, Frijlink HW. Dry powder inhalation: past, present and future. *Expert Opin Drug Deliv* 2017;**14**:499–512.
3. Faulhammer E, Zellnitz S, Wutscher T, Stranzinger S, Zimmer A, Paudel A. Performance indicators for carrier-based DPIs: carrier surface properties for capsule filling and API properties for *in vitro* aerosolisation. *Int J Pharm* 2018;**536**:326–35.
4. Healy AM, Amaro MI, Paluch KJ, Tajber L. Dry powders for oral inhalation free of lactose carrier particles. *Ad Drug Deliver Rev* 2014;**75**:32–52.
5. Zhang XJ, Zhao ZY, Cui YT, Liu F, Huang ZW, Huang Y, et al. Effect of powder properties on the aerosolization performance of nanoporous mannitol particles as dry powder inhalation carriers. *Powder Technol* 2019;**358**:46–54.
6. Floroiu A, Klein M, Krämer J, Lehr CM. Towards standardized dissolution techniques for *in vitro* performance testing of dry powder inhalers. *Dissolution Technol* 2018;**25**:6–18.
7. Kurumaddali A, Christopher D, Sandell D, Strickland H, Morgan B, Bulitta J, et al. Cascade impactor equivalence testing: comparison of the performance of the modified chi-square ratio statistic (mCSRS) with the original CSRS and EMA's average bioequivalence approach. *AAPS Pharm Sci Tech* 2019;**20**:249.
8. Jafar END, Hamed H, Hadi V. Development of dry powder inhaler formulation loaded with alendronate solid lipid nanoparticles: solid-state characterization and aerosol dispersion performance. *Drug Dev Ind Pharm* 2015;**41**:1431–7.
9. Khalili SF, Ghanbarzadeh S, Nokhodchi A, Hamishehkar H. The effect of different coating materials on the prevention of powder bounce in the next generation impactor. *Res Pharm Sci* 2018;**13**:283–7.
10. Longest W, Farkas D, Bass K, Hindle M. Use of computational fluid dynamics (CFD) dispersion parameters in the development of a new DPI actuated with low air volumes. *Pharm Res* 2019;**36**:110.
11. Mitani R, Ohsaki S, Nakamura H, Watano S. Numerical study on particle adhesion in dry powder inhaler device. *Chem Pharm Bull (Tokyo)* 2020;**68**:726–36.
12. Dolovich MB, Kuttler A, Dimke TJ, Usmani OS. Biophysical model to predict lung delivery from a dual bronchodilator dry-powder inhaler. *Int J Pharm X* 2019;**1**:100018.
13. Ahookhosh K, Saidi M, Aminfar H, Mohammadpourfard M, Yaqoubi S. Dry powder inhaler aerosol deposition in a model of tracheobronchial airways: validating CFD predictions with *in vitro* data. *Int J Pharm* 2020;**587**:119599.
14. Meerburg JJ, Andrinopoulou ER, Bos AC, Shin H, van Straten M, Hamed K, et al. Effect of inspiratory maneuvers on lung deposition of tobramycin inhalation powder: a modeling study. *J Aerosol Med Pulm Drug Deliv* 2020;**33**:61–72.
15. Zhang XJ, Cui YT, Liang RF, Wang GL, Yue X, Zhao ZY, et al. Novel approach for real-time monitoring of carrier-based DPIs delivery process *via* pulmonary route based on modular modified Sympatec HELOS. *Acta Pharm Sin B* 2020;**10**:1331–46.
16. Peng TT, Zhang XJ, Huang Y, Zhao ZY, Liao QY, Xu J, et al. Nanoporous mannitol carrier prepared by non-organic solvent spray drying technique to enhance the aerosolization performance for dry powder inhalation. *Sci Rep* 2017;**7**:46517.
17. Zhao ZY, Huang ZW, Zhang XJ, Huang Y, Cui YT, Ma C, et al. Low density, good flowability cyclodextrin-raffinose binary carrier for dry powder inhaler: anti-hygroscopicity and aerosolization performance enhancement. *Expert Opin Drug Deliv* 2018;**15**:443–57.
18. Zhao ZY, Zhang XJ, Cui YT, Huang Y, Huang ZW, Wang GL, et al. Hydroxypropyl-β-cyclodextrin as anti-hygroscopicity agent in amorphous lactose carriers for dry powder inhalers. *Powder Technol* 2018;**358**:29–38.
19. Leung CMS, Tong ZB, Zhou Q, Chan JGY, Tang P, Sun S, et al. Understanding the different effects of inhaler design on the aerosol performance of drug-only and carrier-based DPI formulations. Part 1: grid structure. *AAPS J* 2016;**18**:1159–67.
20. Hertel N, Birk G, Scherliess R. Particle engineered mannitol for carrier-based inhalation—a serious alternative?. *Int J Pharm* 2020;**577**:118901.
21. Kaialy W, Alhalaweh A, Velaga SP, Nokhodchi A. Influence of lactose carrier particle size on the aerosol performance of budesonide from a dry powder inhaler. *Powder Technol* 2012;**227**:74–85.
22. Gilani K, Darabi M, Barghi M. Influence of formulation variables and inhalation device on the deposition profiles of cromolyn sodium dry powder aerosols. *Daru J Pharm Sci* 2004;**12**:89–94.
23. Donovan MJ, Smyth HDC. Influence of size and surface roughness of large lactose carrier particles in dry powder inhaler formulations. *Int J Pharm* 2010;**402**:1–9.
24. Martin S, Silvio S. Numerical analysis of carrier particle motion in a dry powder inhaler. *J Fluid Eng* 2015;**138**:46–54.
25. Kho K, Hadinoto K. Dry powder inhaler delivery of amorphous drug nanoparticles: effects of the lactose carrier particle shape and size. *Powder Technol* 2013;**233**:303–11.
26. Donovan MJ, Kim SH, Raman V, Smyth HD. Dry powder inhaler device influence on carrier particle performance. *J Pharm Sci* 2012;**101**:1097–107.
27. Huang Y, Huang ZW, Zhang XJ, Zhao ZY, Zhang X, Wang KX, et al. Chitosan-based binary dry powder inhaler carrier with nanometer roughness for improving *in vitro* and *in vivo* aerosolization performance. *Drug Deliv Transl Re* 2018;**8**:1274–88.
28. Renner N, Steckel H, Urbanetz N, Scherließ R. Nano- and microstructured model carrier surfaces to alter dry powder inhaler performance. *Int J Pharm* 2017;**518**:20–8.
29. Tan BMJ, Chan LW, Heng PWS. Characterizing the surface roughness length scales of lactose carrier particles in dry powder inhalers. *Mol Pharm* 2018;**15**:1635–42.
30. Littringer EM, Mescher A, Schroettner H, Achelis L, Walzel P, Urbanetz NA. Spray dried mannitol carrier particles with tailored surface properties—the influence of carrier surface roughness and shape. *Eur J Pharm Biopharm* 2012;**82**:194–204.
31. Zellnitz S, Schroettner H, Urbanetz NA. Surface modified glass beads as model carriers in dry powder inhalers—influence of drug load on the fine particle fraction. *Powder Technol* 2014;**268**:377–86.
32. Singh DJ, Jain RR, Soni PS, Abdul S, Darshana H, Gaikwad RV, et al. Preparation and evaluation of surface modified lactose particles for improved performance of fluticasone propionate dry powder inhaler. *J Aerosol Med Pulm Drug Deliv* 2015;**28**:254–67.
33. Freeman R. Measuring the flow properties of consolidated, conditioned and aerated powders—a comparative study using a powder rheometer and a rotational shear cell. *Powder Technol* 2007;**174**:25–33.
34. Gnagne EH, Petit J, Gaiani C, Scher J, Amani GN. Characterisation of flow properties of foutou and foufou flours, staple foods in West Africa, using the FT4 powder rheometer. *J Food Meas Charact* 2017;**11**:1128–36.
35. Faulhammer E, Wahl V, Zellnitz S, Khinast JG, Paudel A. Carrier-based dry powder inhalation: impact of carrier modification on capsule filling processability and *in vitro* aerodynamic performance. *Int J Pharm* 2015;**491**:231–42.
36. Andrea E, Marina C, Ciro C, Daniela R, Claudio C, Roberto B, et al. Multivariate data analysis to assess dry powder inhalers performance from powder properties. *Powder Technol* 2016;**301**:830–8.
37. Shalash AO, Khalafallah NM, Molokhia AM, Elsayed MM. The relationship between the permeability and the performance of carrier-

based dry powder inhalation mixtures: new insights and practical guidance. *AAPS PharmSciTech* 2017;**19**:912−22.
38. Fu X, Huck D, Makein L, Armstrong B, Willen U, Freeman T. Effect of particle shape and size on flow properties of lactose powders. *Particuology* 2012;**10**:203−8.
39. Kou X, Wereley ST, Heng PW, Chan LW, Carvajal MT. Powder dispersion mechanisms within a dry powder inhaler using microscale particle image velocimetry. *Int J Pharm* 2016;**514**:445−55.
40. Le VN, Robins E, Flament MP. Air permeability of powder: a potential tool for dry powder inhaler formulation development. *Eur J Pharm Biopharm* 2010;**76**:464−9.
41. Wirth KE, Linsenbühler M. Electrostatically supported mixing of fine grained particles. *China Particuol* 2005;**3**:94−8.
42. Hoppentocht M, Hagedoorn P, Frijlink HW, de Boer AH. Technological and practical challenges of dry powder inhalers and formulations. *Adv Drug Deliv Rev* 2014;**75**:18−31.
43. Begat P, Morton DA, Staniforth JN, Price R. The cohesive-adhesive balances in dry powder inhaler formulations I: direct quantification by atomic force microscopy. *Pharm Res* 2004;**21**:1591−7.
44. Tan SB, Newton JM. Influence of capsule dosator wall texture and powder properties on the angle of wall friction and powder-wall adhesion. *Int J Pharm* 1990;**64**:227−34.
45. Zhou QT, Tong Z, Tang P, Citterio M, Yang R, Chan HK. Effect of device design on the aerosolization of a carrier-based dry powder inhaler—a case study on Aerolizer Foradile. *AAPS J* 2013;**15**:511−22.
46. Frijlink HW, De Boer AH. Dry powder inhalers for pulmonary drug delivery. *Expert Opin Drug Deliv* 2004;**1**:67−86.
47. Lam KK, Newton JM. Influence of particle size on the adhesion behaviour of powders, after application of an initial press-on force. *Powder Technol* 1992;**73**:117−25.
48. Marriott C, Litt M. The effect of additives on the rheological properties of tracheal mucus. *J Pharm Pharmacol* 1978;**30**:9.
49. Tang P, Kwok PCL, Tong Z, Yang R, Raper JA, Chan HK. Does the United States Pharmacopeia throat introduce de-agglomeration of carrier-free powder from inhalers?. *Pharm Res* 2012;**29**:1797−807.
50. Ruzycki CA, Martin AR, Finlay WH. An exploration of factors affecting *in vitro* deposition of pharmaceutical aerosols in the alberta idealized throat. *J Aerosol Med Pulm Drug Deliv* 2019;**32**:405−17.
51. Qiu Y, Man RCH, Liao Q, Kung KLK, Chow MYT, Lam JKW. Effective mRNA pulmonary delivery by dry powder formulation of PEGylated synthetic KL4 peptide. *J Control Release* 2019;**314**:102−15.
52. Lababidi N, Ofosu Kissi E, Elgaher WAM, Sigal V, Haupenthal J, Schwarz BC, et al. Spray-drying of inhalable, multifunctional formulations for the treatment of biofilms formed in cystic fibrosis. *J Control Release* 2019;**314**:62−71.